Supporting Information

Revealing Grain Dependent Glucose Oxidation Pathways on Gold with Scanning Electrochemical Cell Microscopy

Anju Singh[a†], Anuradha Irugalbandara[a†], Moonika Widjajana[b,c], Jiancheng Lin[c], Levi Tegg[d], Isaac J. Gresham[a], Kourosh Kalantar-Zadeh[b,c], Minkyung Kang*[a]

[a] School of Chemistry, The University of Sydney, NSW 2006, Australia.

[b] School of Chemical and Biomolecular Engineering, University of Sydney, NSW 2006, Australia;

[c] School of Chemical Engineering, The University of New South Wales, Sydney (UNSW), NSW 2052, Australia.

[d] School of Aerospace, Mechanical and Mechatronic Engineering, The University of Sydney, NSW 2006, Australia.

[†] These authors contributed equally to this work

Corresponding e-mail: minkyung.kang@sydney.edu.au (M.K.)

Contents

S1. Materials and Methods

S1.1 Preparation of the working Electrodes

In this study, gold nugget was used as a working electrode, a fine gold chip (0.29 mm thick, 99.99+% purity, Argor-Heraeus, Switzerland) was melted using a butane torch (Duratech, Taiwan) to form a rounded shape at the end of the gold piece[1,2].The molten gold was then rapidly quenched in deionised water at room temperature. After cooling, the gold ball was gently compressed and cleaned. This melting, quenching, and reshaping process was repeated until the desired nugget morphology was achieved. The resulting gold nuggets were further cleaned sequentially with isopropanol, acetone, and deionised water, followed by drying. Finally, the nuggets were plasma cleaned using a microprocessor-controlled benchtop plasma cleaner (HPT-200 Henniker Plasma, UK) to remove any oxidised surface layers prior to use in SECCM measurements. The gold nugget was further characterised by SEM (Fig. 1a) to visualise the grain structure, and AFM was used to examine the surface topography (Fig. S2).

S1.2 Nanopipettes, Quasi-Reference/ Counter Electrodes, and Electrolytes

Nanopipettes were fabricated from borosilicate glass capillaries (World Precision Instruments, USA; capillary outer diameter: 1.2 mm, inner diameter, 0.68 mm; and length, 100 mm) with a laser puller (Sutter Instruments Co. P-2000, US). The pulling parameters were as follows: line 1 with HEAT 360, FIL 3, VEL 40, DEL 220, and PUL−0 and line 2 with HEAT 355, FIL 4, VEL 40, DEL 220, and PUL 120. The nanopipette tip opening was ~700 nm in diameter (Fig. S1).

AgCl-coated Ag (Ag/AgCl) quasi reference counter electrodes (QRCEs) were fabricated by cathodic polarisation of a silver (Ag) wire (0.125 mm in diameter, 99.99+%, Goodfellow, UK) in saturated KCl solution for 10-15 mins [1]. The resulting AgCl-coated Ag wires were calibrated in the solution against a commercial leakless Ag/AgCl reference electrode (3.4 mol/L KCl,

ET072, eDAQ, Australia), yielding a stable offset potential of 140 ± 5 mV. Accordingly, all electrochemical potentials reported in this study are referenced to the commercial Ag/AgCl (3.4 mol/L KCl) electrode, hereafter referred to as Ag/AgCl. Freshly prepared 0.1 M D-Glucose Anhydrous (99.99%, Chem-Supply Pty Ltd., Australia) in 0.5 M phosphate buffer (pH 7.4) was used as the electrolyte for SECCM measurements.

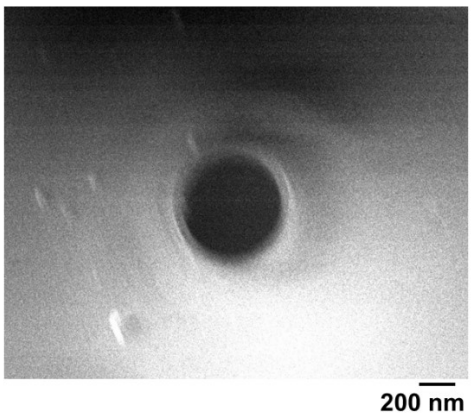

Figure S1. SEM image of borosilicate glass capillaries pipette tip (700 nm) used in scanning during SECCM measurements.

S1.3 Local Electrochemical Characterisation: SECCM

A custom-built SECCM workstation was employed for all experiments[3]. The nanopipette probe (~700 nm diameter) was filled with the solution and equipped with an Ag/AgCl QRCE positioned ~1 cm from the tip [4]. The probe was mounted on piezoelectric linear stages (Newport M-423 series, US), allowing coarse movement along the x, y, and z axes. Tip positioning over the gold surface was guided by optical visualisation with a camera (Axiocam, Carl Zeiss Microscopy GmbH, Germany) equipped with a Compact TL 6× telecentric lens (Edmund Optics, UK). The gold nugget or film serving as the working electrode was cantered inside a polypropylene environmental cell (HPL 931, Lock & Lock, South Korea; 74 x 43 mm cm, 100 ml volume) allowing atmospheric control under humidified argon[5]. The cell was mounted on an x−y piezoelectric positioner (Nano-3D200, Mad City Labs Inc., US). The humidified gas

was supplied via a 6 mm Pneumatic Push In Air Fittings (RS Pro, UK) with nylon tube. The entire assembly—including the environmental cell, stages, camera, and collimated illumination—was enclosed in a customised Faraday cage (The University of Sydney, Science Design & Prototyping, Australia) for electrical shielding, mounted on a Minus K negative stiffness vibration isolator platform (minus K Technology, US), and placed on an optical tabletop (RS 2000, Newport, US) to minimize vibrations. Data acquisition and instrument control were performed using an FPGA card (USB-7856, National Instruments, US) operated via LabVIEW 2021 interface software (National Instruments) running on Warwick electrochemical scanning probe microscopy (WEC-SPM) software (www.warwick.ac.uk/electrochemistry/wec-spm).

SECCM was operated in hopping mode over a 180 × 180 μm² area with a hopping distance of 5 μm, with approach rate of 5 μm s^{-1} (i.e., vertical probe movement) and scan rate of 10 μm/s (i.e., lateral probe movement). Cyclic voltammetry (CV) was performed at each predefined location (pixel) where the nanopipette meniscus contacted the gold surface[6]. At each landing, an independent CV was recorded. This point-by-point approach enabled spatially resolved GOR at the gold surface. The substrate current was measured using a current amplifier (DLPCA-200, FEMTO, Germany), and the potential was applied to the QRCE in the SECCM probe relative to the FPGA card. A triangular waveform was then applied from −0.5 to 1.2 V and back to 0.5 V at a scan rate of 0.1 Vs^{-1}. The nanopipette was subsequently retracted by 5 μms^{-1} before moving to the next pixel to repeat the procedure. After scanning, droplet footprints were imaged via scanning electron microscopy (SEM) equipped with electron backscatter diffraction (EBSD), revealing variations in the wetted (effective) working electrode area as well as crystal orientation on polycrystalline gold. Raw data were processed in MATLAB R2024b (MathWorks, US) to analysed voltammograms, current density (mA cm^{-2}) maps, and movies.

S1.4 Surface morphology characterisation

S1.4.1 EBSD

EBSD measurements were performed on the samples after SECCM analysis using a Zeiss Ultra field emission SEM (FE-SEM, Zeiss, Germany) equipped with an Oxford Instruments Symmetry EBSD detector (UK). EBSD maps were collected at 30 kV accelerating voltage, 5 ms exposure with a 120 μm aperture, while the sample was tilted 70° towards the detector. The raw EBSD data were first acquired and indexed using AZtec software (Oxford Instruments, UK), which is integrated with the instrument control. The AZtecICE module, and a custom MATLAB code and MTEX were applied for initial data handling and for EBSD pattern processing, followed by AZtecCrystal Advanced (Channel 5 software) for post-acquisition analysis. Grain boundary networks and average grain parameters relevant to correlation with the SECCM data were extracted from the final processed datasets.

S1.4.2 AFM

AFM measurements were carried out as a complementary analysis to quantify the surface roughness of the samples using a Dimension Nexus AFM (Bruker, USA) equipped with a NanoScope 6 controller. Imaging was performed in tapping mode under ambient conditions using silicon cantilevers (TESPA-V2) with a nominal tip radius of <7 nm, a resonance frequency of ~320 kHz, and a force constant of 42 N m^{-1}, operated using the NanoScope Tapping ScanAsyst Plus mode. AFM topography maps were acquired over a scan area of 90 μm × 90 μm at a scan rate of 0.25 Hz. The raw height images were processed using NanoScope Analysis 3.0 and Gwyddion software, where plane leveling was applied to remove background tilt prior to analysis. Quantitative surface parameters, including the root-mean-square (RMS) roughness, were extracted from the processed datasets. The RMS roughness of the sample surface was determined to be 4.26 nm.

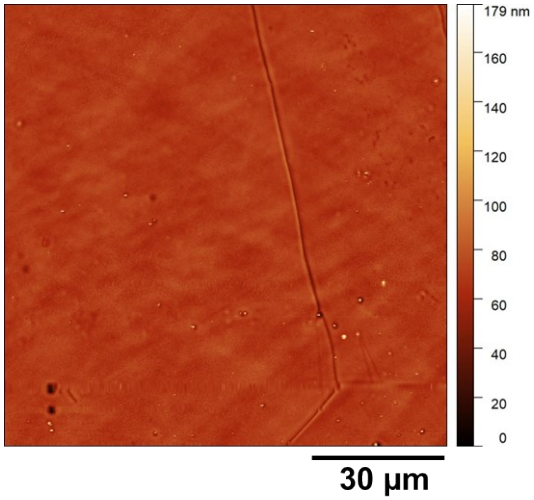

Figure S2. AFM topography of the gold nugget, used as the working electrode in SECCM measurements, acquired over a 90 × 90 µm² area at a scan rate of 0.25 Hz.

S2. Electrochemical Movie Captions

S2.1 Movie S1: Electrochemical (potentiodynamic) movie of voltammetric SECCM measurements performed on a gold *nugget* under Ar, corresponding to the results presented in Fig. 3 of the main text. Scanning protocol, as described in the Methods section, was employed for scan acquisition. The movie displays a sequence of electrochemical frames representing current maps of the gold *nugget* as the surface potential was swept from –0.2 V to 1.2 V vs Ag/AgCl. The total scanned area was 180 μm, comprising 400 cyclic voltammetry measurements across 9 distinct grains.

S2.2 Movie S2: Electrochemical (potentiodynamic) movie of voltammetric SECCM measurements on a gold *nugget* under Ar, corresponding to the results presented in Fig. 3 of the main text. Scanning protocol, as described in the Methods section was used for the scan acquisition. The movie shows a series of electrochemical frames that correspond to current maps of the gold *nugget* as the potential, E_{surf}, is swept from -0.1 V to 1.2 V vs Ag/AgCl. The total scanned area was 180 μm, comprising 1521 measurements recorded across 10 grains.

S2.3 Movie S3: Electrochemical (potentiodynamic) movie of voltammetric SECCM measurements on a gold *nugget* under Ar, corresponding to the results presented in result and discussion Fig. 4. Scanning protocol, as described in the Methods section was used for the scan acquisition. The movie shows a series of electrochemical frames that correspond to current maps of the gold *nugget* as the potential, E_{surf}, is swept from -0.1 V to 1.2 V *vs* Ag/AgCl. The total scanned area was 180 μm, comprising 868 measurements recorded across 6 grains. The movie includes the first voltammetric cycle recorded at a single location on the Au surface during the SECCM experiment.

S2.4 Movie S4: Electrochemical (potentiodynamic) movie of voltammetric SECCM measurements on a gold *nugget* under Ar, corresponding to the results presented in result and

discussion Fig. 4. Scanning protocol, as described in the Methods section was used for the scan acquisition. The movie shows a series of electrochemical frames that correspond to current maps of the gold *nugget* as the potential, E_{surf}, is swept from -0.1 V to 1.2 V *vs* Ag/AgCl. The total scanned area was 180 μm, comprising 868 measurements recorded across 6 grains. The movie includes the second voltammetric cycle recorded at a single location on the Au surface during the SECCM experiment.

S3. Overall Data Analysis and Coding Workflow

All coding, data processing, and visualisation steps were performed for *Glucose Scan 1*, *Glucose Scan 2*, and *Glucose Scan 3*, separately using custom MATLAB scripts created in this study.

Table S1 - The specific voltages considered in each scan were determined by identifying characteristic peak positions from the overall cyclic voltammogram of each scan, representing key electrochemical processes.

Glucose Scan 1		**Glucose Scan 2**		**Glucose Scan 3**	
Potential (V)	CV Direction	Potential (V)	CV Direction	Potential (V)	CV Direction
0.24	Forward	0.88	Forward	0.36	Forward
0.83	Forward	0.18	Reverse	0.92	Forward
0.15	Reverse	0.40	Reverse	0.02	Reverse
−0.10	Reverse	−0.09	Reverse	0.18	Reverse
0.39	Reverse			0.40	Reverse

S3.1 Extraction of Individual Droplet Areas for SECCM Electrochemical maps

A custom MATLAB workflow was developed to calculate the footprint area of individual droplets within each scan. Image of droplet footprint obtained from SEM analysis were imported and scaled using a known pixel-to-length calibration, allowing all measurements to be expressed in micrometre units. Droplet boundaries were identified through a manually adjustable thresholding interface based on Otsu's method.

Following thresholding, the binary masks were refined using morphological operations, including noise removal, hole filling, and edge smoothing. The segmented droplets were then labelled and analysed using the *regionprops* function to extract their respective areas.

For scans with uniformly distributed droplets, an automated nearest-neighbour algorithm was applied to assign droplet numbering. In cases of irregular droplet placement, manual numbering was performed through an interactive graphical interface. The resulting droplet indices and corresponding areas (μm²) were exported to Excel files for subsequent normalisation of current data and generation of current density Electrochemical maps.

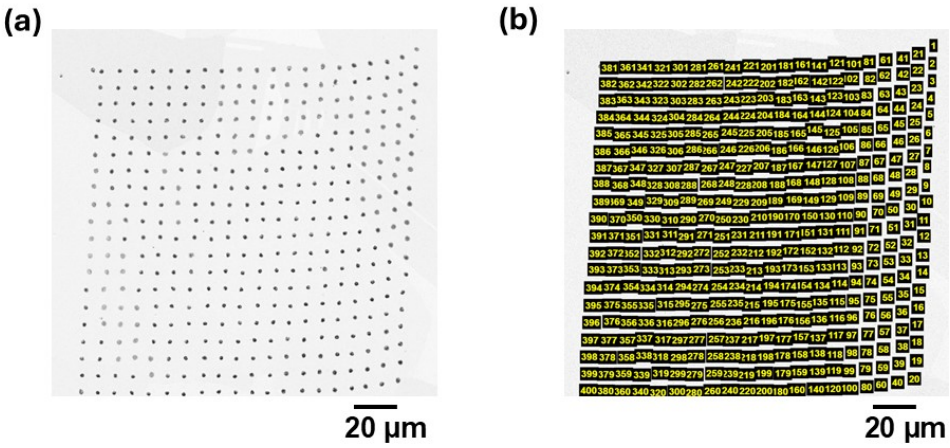

Figure S3 (a) SEM image of Glucose Scan 1; (b) Corresponding processed image showing the numbered droplet areas.

S3.2 Generation of Current Density Electrochemical Maps

Then, using a MATLAB script, frames were plotted separately for the specific voltages listed in Table S1, using the Excel file containing the individual droplet areas and the mean droplet area for each scan.

S3.3 Generation of Absolute Difference Electrochemical Maps

A custom MATLAB script was developed to generate the absolute difference maps of current density between two electrochemical maps corresponding to the same potential. The electrochemical map data were extracted from .fig files, converted to numerical matrices, and aligned to ensure identical grid dimensions. The absolute difference in current density between the two datasets was then calculated on a pixel-by-pixel basis to visualize spatial variations

between the electrochemical maps. The resulting reduction maps were plotted using a red scale colormap.

S4. Correlative SECCM-EBSD image analysis protocol

S4.1 EBSD Map Generation and Determination of Grain Orientations

A custom MATLAB script was developed to generate the EBSD orientation map and extract crystallographic information from the scanned region. The EBSD data file (.ctf) was imported assuming cubic crystal symmetry, and grains were identified using a misorientation threshold of 2°. Only large grains with a size exceeding 100 pixels were considered to enhance the precision of subsequent analysis.

For each grain, the script computed Euler angles and determined the mean orientation. The mean orientation matrix was used to transform the reference sample direction (z-axis) into the crystal frame, allowing determination of the corresponding crystallographic planes as fractional Miller indices (hkl). To convert these fractional indices to physically meaningful integer Miller indices, a scaling optimisation routine was applied. Each fractional vector was multiplied by scaling factors ranging from 0.3 to 2.0 in increments of 0.01. For each scaled vector, the components were rounded to the nearest integer, and the scaling factor that minimised the relative deviation between the scaled fractional vector and the rounded integers was selected. The resulting integer vector was then simplified by dividing all components by their greatest common divisor to remove redundancy. These modified Miller indices were manually validated by inspecting the scaling factors to ensure accurate representation of the crystallographic orientation.

The final output included the grain ID, Euler angles, fractional and modified Miller indices, and scaling factors, which were exported as a CSV file. The EBSD map was plotted with overlaid grain boundaries, and large grains were labelled with their corresponding grain ID and Miller indices for visualisation.

S4.2 Correlation of Droplet Positions with Grains via Area-Based Mapping

A custom MATLAB code developed to correlate each individual droplets to grains via area-based mapping. Band contrast maps were plotted with overlaid grain boundaries, and large grains were labelled with their respective IDs. Droplet positions and boundaries were extracted from a previously generated MATLAB figure containing droplet numbering.

To align the droplet map with the EBSD map, control points were manually selected on both images, and an affine transformation was applied to warp the droplet coordinates and boundaries onto the EBSD coordinate system. Droplets were then allocated to large grains based on maximum overlap area with grain regions. For droplets not overlapping any grain, the nearest grain boundary was used for assignment. Droplet-to-grain mappings were recorded, and results were exported as a correlation table (Excel file) including grain IDs, Miller indices, colour, and droplet IDs.

Finally, IPF maps were plotted with color-coded grains and overlaid droplets. Visualisations included both numbered droplets and color-coded droplets (without numbering). The Excel file was manually inspected and corrected, to ensure accurate allocation of droplets to their respective grains by cross-checking the figures.

S4.3 Grain Boundary Detection and Visualisation from SECCM Electrochemical maps

A custom MATLAB code developed in this work was used to visualise grain boundaries and assign crystallographic information to Electrochemical maps. Grayscale Electrochemical maps were generated from previously processed SECCM data corresponding to the voltages listed in Table S1. The Electrochemical maps input to this section were calculated using individual droplet areas. The MATLAB workflow began by loading the Electrochemical maps figure and converting it into grayscale for uniform visualisation.

Grain properties—including droplet IDs, colour codes, and Miller indices—were extracted from the Excel file generated in the previous section. Each pixel in the Electrochemical maps was mapped to its corresponding grain, colour, and Miller index. Grain boundaries were identified and drawn by comparing the Miller indices of neighbouring pixels, allowing clear visual distinction of crystallographic regions within the grayscale Electrochemical maps.

S4.4 Cyclic Voltammetry Analysis and Detection of Grains with Similar Electrochemical Responses

A custom MATLAB code was developed to analyse cyclic voltammograms (CVs) for individual grains. The current–voltage matrices used in this step were obtained from the SECCM scan data, while the droplet footprint areas were determined in the initial stage of the workflow.

The MATLAB script imported the voltage and current density matrices together with the grain information file containing droplet IDs and their respective Miller indices. For each grain, CVs of all associated droplets were plotted individually, followed by an averaged CV curve representing the mean electrochemical response of that grain. To ensure consistency, droplets exhibiting abnormally high current densities were excluded from the analysis.

After generating individual grain plots, grains exhibiting similar electrochemical responses were detected by comparing the shapes and peak characteristics of their CVs. They were grouped manually, and combined plots were generated to visualize the mean cyclic voltammograms of multiple selected grains within a single frame.

S5. Normalisation of SECCM Electrochemical Map by Individual Droplet Areas (Figure 2)

Glucose Scan 1

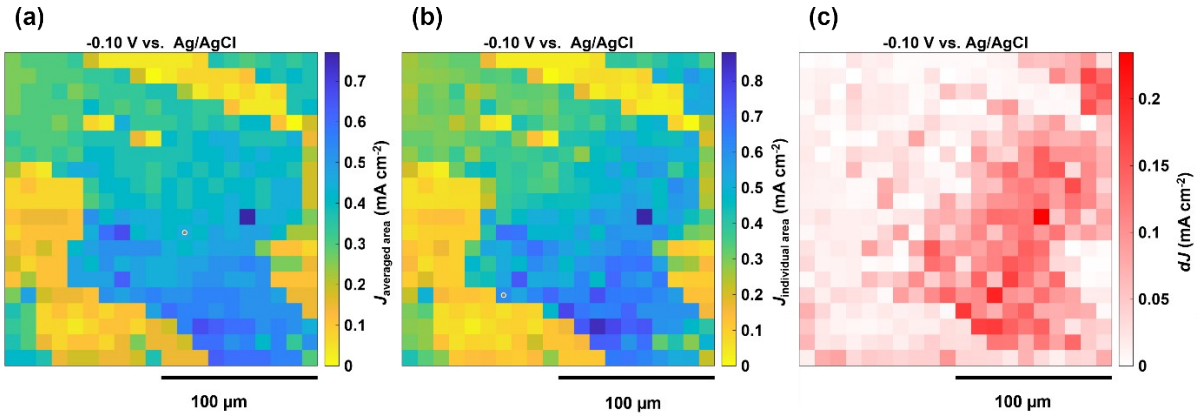

Figure S4 (a) Electrochemical map at -0.10 V (Glucose Oxidation-I) calculated using the mean droplet area; (b) Electrochemical map at -0.10 V calculated using individual droplet areas; (c) Absolute difference of current density in two Electrochemical maps at -0.10 V ($dJ = |J_{\text{averaged area}} - J_{\text{individual area}}|$).

Grain-dependent current density variations are clearly visible in both (a) and (b). However, when the mean droplet area is used, the current density response appears higher than the actual values in electrochemically more active grain regions, as evident in (c).

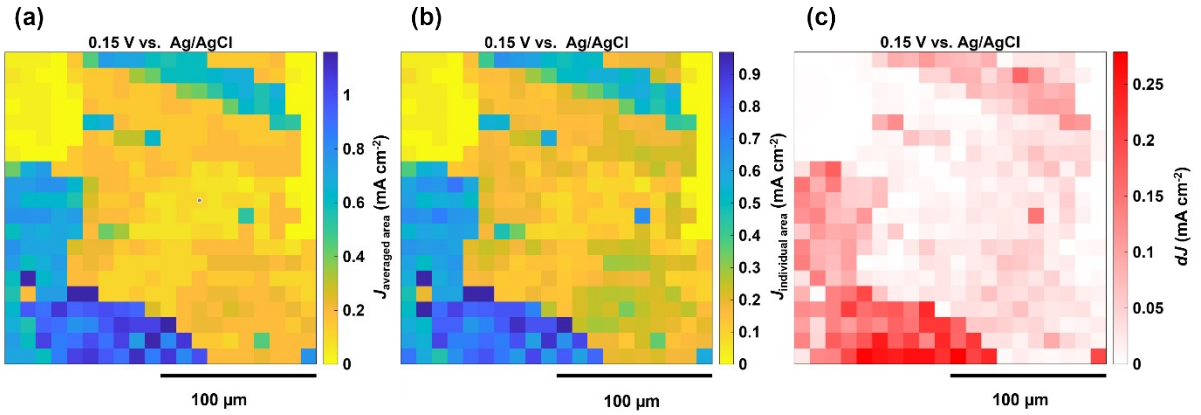

Figure S5 (a) Electrochemical map at 0.15 V (Glucose Oxidation-II) calculated using the mean droplet area; (b) Electrochemical map at 0.15 V calculated using individual droplet areas; (c) Absolute difference of current density in two Electrochemical maps at 0.15 V ($dJ = |J_{\text{averaged area}} - J_{\text{individual area}}|$).

Grain-dependent current density variations are clearly visible in both (a) and (b). Similar to Fig. 2, when the mean droplet area is used, the current density response appears higher than the actual values in electrochemically more active grain regions, as evident in (c).

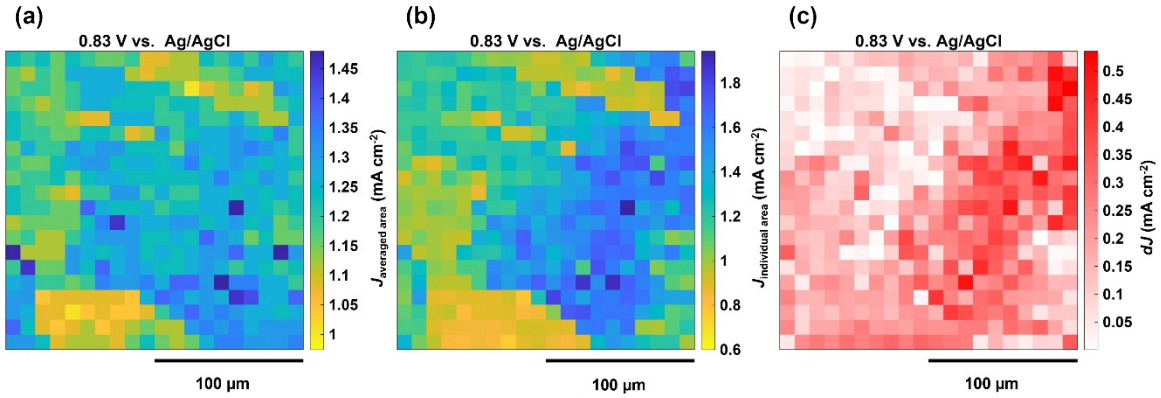

Figure S6 (a) Electrochemical map at 0.83 V (gold oxide reduction) calculated using the mean droplet area; (b) Electrochemical map at 0.83 V calculated using individual droplet areas; (c) Absolute difference of current density in two Electrochemical maps at 0.83 V ($dJ = |J_{\text{averaged area}} - J_{\text{individual area}}|$).

The overall current density response is significantly higher during gold oxidation. In (a), grain-dependent current density variations are less apparent, while in (b), these variations are clearly visible. As shown in (c), the absolute difference is not grain-dependent, with higher magnitude values compared to those in Fig. 2 and 3.

Glucose Scan 2

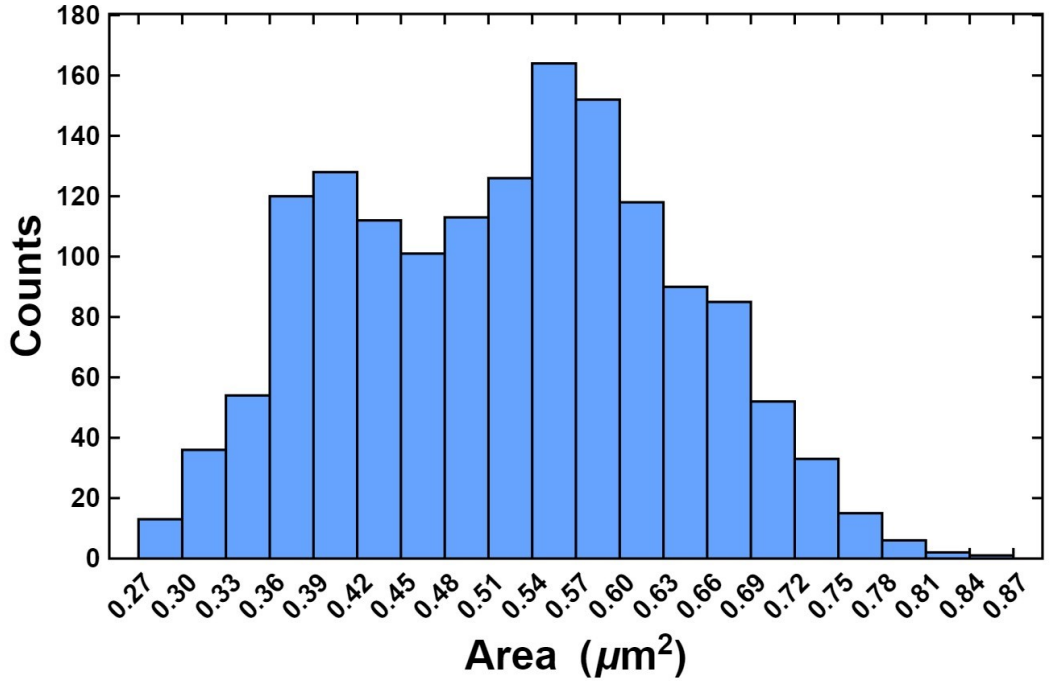

Figure S7 Droplet area distribution histogram for Glucose Scan 2. Areas ranged from 0.27 to 0.85 µm² with an averaged area of 0.52 µm² and a standard deviation of 0.11 µm².

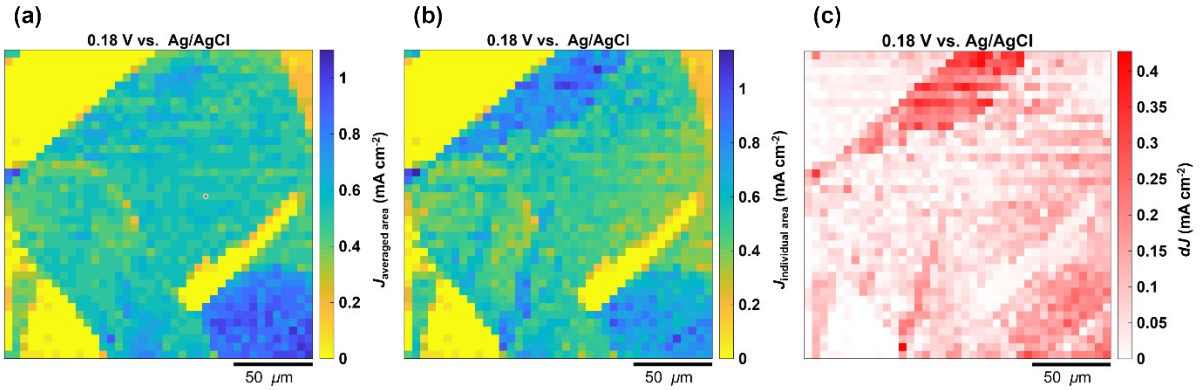

Figure S8 (a) Current density Electrochemical map at 0.18 V (gold oxide reduction) calculated using the mean droplet area; (b) Electrochemical map at 0.18 V calculated using individual droplet areas; (c) Absolute difference of current density in two Electrochemical maps at 0.18 V ($dJ = |J_{\text{averaged area}} - J_{\text{individual area}}|$).

Grain-dependent current density variations are clearly visible in both (a) and (b), with current density values remaining within a similar range. However, slight deviations can be observed in specific regions, and more pronounced grain-dependent variations are evident in (b), as further highlighted in (c).

S6. Glucose Scan 1: Activity Map, EBSD image, SEM image of areas scanned with SECCM

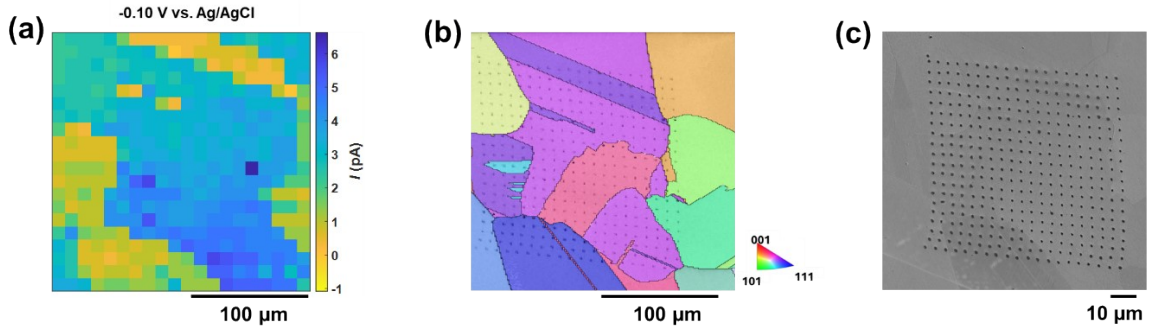

Figure S9. Results of SECCM scan 1 on gold *nugget*. (a) Electrochemical image extracted from potentiodynamic SECCM movie (Movie S1) at potential -1.02 V vs. Ag/AgCl across the different grains (b) co-located EBSD map, (c) SEM image of the same scanned area, showing different size footprints of glucose droplets during the Glucose Scan 1 SECCM measurement (Section 2.3).

S7. Glucose Scan 1 & Scan2: Gold Oxidation and Gold Oxide Reduction Electrochemical Map

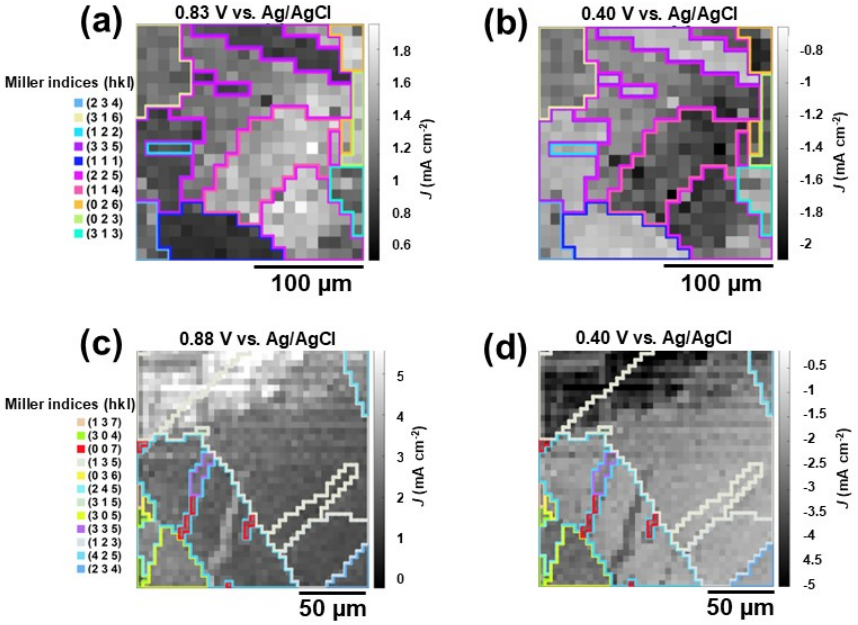

Figure S10. SECCM results obtained on a gold nugget. (a) Electrochemical image extracted from the potentiodynamic SECCM movie (Movie S1 and Movie S2) at potential 0.83 V vs Ag/AgCl, and 0.40V vs Ag/AgCl, showing activity across different grains identified from the co-located EBSD map (highlighted by boxes). Scan 1: (a) Gold oxidation observed at 0.83 V vs Ag/AgCl (forward scan), and (b) reduction of gold oxide at 0.40 V vs Ag/AgCl (reverse scan), and Scan 2: (a) Gold oxidation observed at 0.88 V vs Ag/AgCl (forward scan), and (b) reduction of gold oxide at 0.40 V vs Ag/AgCl (reverse scan), (Section 2.3).

S8. Effect of repeated CV cycling on grain-dependent GOR activity (*Glucose Scan 3*)

Two consecutive SECCM CVs at a single location on the gold nugget were used to evaluate how repeated oxidation–reduction cycles [7] influence glucose oxidation (GOR). Six grains were analysed: Au (334) and Au (344) displaying Glucose Oxidation–II, Au (124) and Au (217) exhibiting Glucose Oxidation–I (Fig. S11), and Au (227) and Au (215), which showed distinct electrochemical responses (Fig. S12). In cycle 1, Glucose Oxidation–II peaks on Au (334) and Au (344) appeared at ~0.17 V vs Ag/AgCl. Cycle 2 CVs showed increased currents due to partial oxide/adsorbate removal. This enhancement is evident in the corresponding electrochemical maps (Fig. S11b, S11e) and is consistent with previous reports on electrochemical activation of gold electrodes [8,9].

For grains exhibiting Glucose Oxidation–I behaviour (Au (124) and Au (217)), an oxidation feature in the 0.27–0.40 V vs Ag/AgCl range, absent in cycle 1 (Fig. S11c), emerged in cycle 2 with a current density of ~0.06 mA cm^{-2} (Fig. S11f). A comparable enhancement was observed for Glucose Oxidation–II on Au (334) and Au (344). Specifically, in cycle 1 (Fig. S11c), a broad oxidation peak spanning 0.15–0.47 V vs Ag/AgCl reached ~0.13 mA cm^{-2} at 0.34 V vs Ag/AgCl, whereas in cycle 2 (Fig. S11f) the peak shifted to more negative potentials (0.05–0.38 V vs Ag/AgCl) and increased to ~0.43 mA cm^{-2} at 0.19 V vs Ag/AgCl during the forward scan. In the reverse scan of cycle 2, a pronounced oxidation peak was observed at 0.17 V vs Ag/AgCl with a current density of ~1.22 mA cm^{-2}, which increased slightly to ~1.61 mA cm^{-2} at 0.15 V vs Ag/AgCl upon repeat scanning, while the peak potential and shape remained largely unchanged. Grains Au (227) and Au (215) exhibited distinct CV features in the −0.12 to 0.26 V vs Ag/AgCl range with current densities up to ~0.19 mA cm^{-2} (Fig. S12), but similarly showed enhanced activity with successive cycles, confirming surface activation across different grain indices.

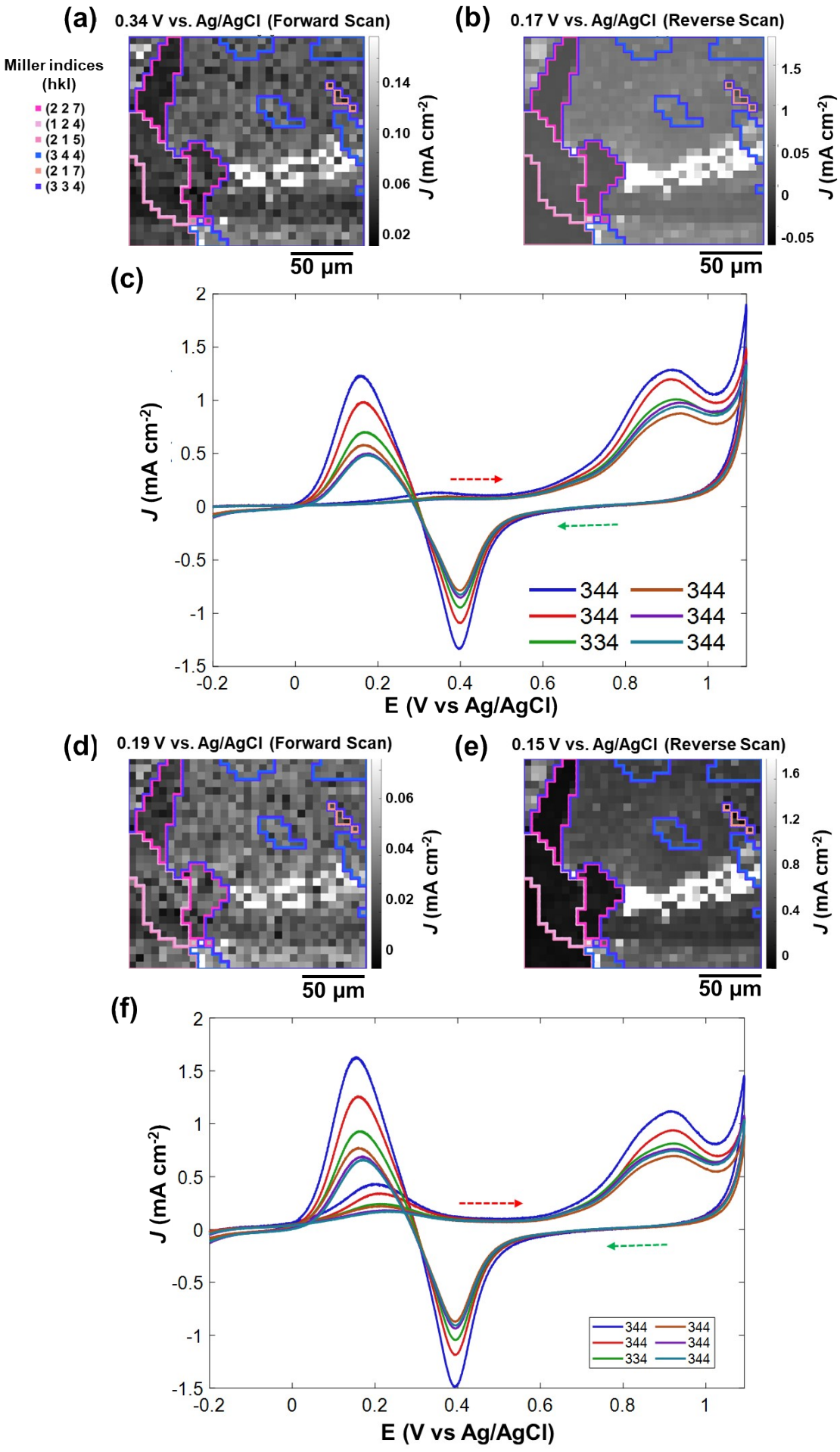
(a)
0.34 V vs. Ag/AgCl (Forward Scan)
Miller indices (hkl)
(2 2 7)
(1 2 4)
(2 1 5)
(3 4 4)
(2 1 7)
(3 3 4)
0.14
0.10
0.06
0.02
J (mA cm-2)
50 µm
(b)
0.17 V vs. Ag/AgCl (Reverse Scan)
1.5
1
0.05
0
-0.05
J (mA cm-2)
50 µm
(c)
J (mA cm-2)
E (V vs Ag/AgCl)
344
344
344
344
334
344
(d)
0.19 V vs. Ag/AgCl (Forward Scan)
0.06
0.04
0.02
0
J (mA cm-2)
50 µm
(e)
0.15 V vs. Ag/AgCl (Reverse Scan)
1.6
1.2
0.8
0.4
0
J (mA cm-2)
50 µm
(f)
J (mA cm-2)
E (V vs Ag/AgCl)
344
344
344
344
334
344

Figure S11. Two consecutive cyclic voltammograms recorded at a single point on the gold nugget surface during SECCM measurements. The scan direction is indicated by dashed arrows—red (left to right) for the forward scan and green (right to left) for the reverse scan. Spatially resolved equipotential snapshot images extracted from Movie S3 (cycle 1), Movie S4 (cycle 2) illustrate the SECCM electrochemical maps for (a) 0.34 V vs Ag/AgCl (forward) and (b) 0.17 V vs Ag/AgCl (reverse); (d) 0.19 V vs Ag/AgCl (forward) and (e) 0.15 V vs Ag/AgCl (reverse) in Cycle 2. The corresponding cyclic voltammograms are shown in (c) for Cycle 1 and (f) for Cycle 2. Note that the colours in the CVs are not following IPF key colour. It is only for distinguishing different grain with the same grain orientation within the scan.

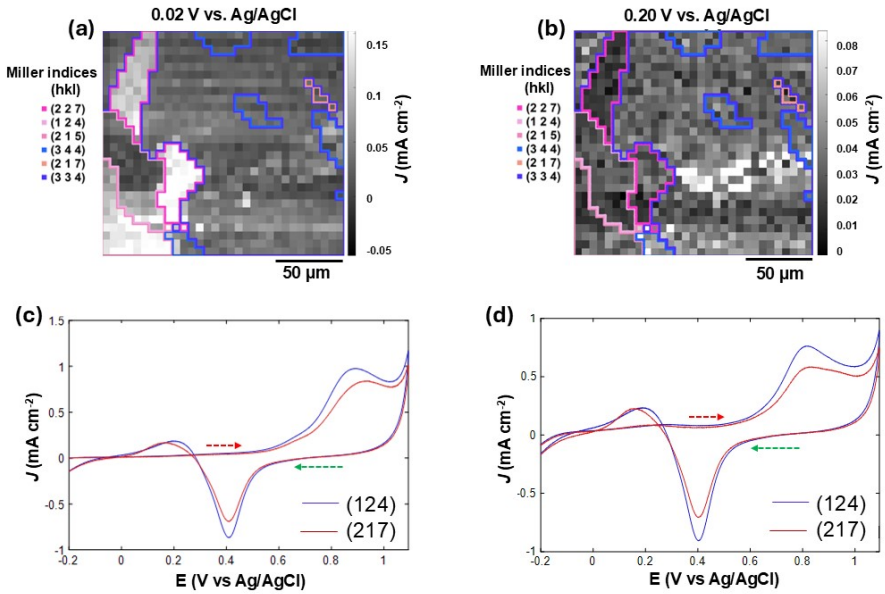

Figure S12. Two consecutive cyclic voltammograms recorded at a single point on the gold nugget surface using SECCM. The scan direction is indicated by dashed arrows—red (left to right) for the forward scan and green (right to left) for the reverse scan. Glucose oxidation-I appears at approximately 0.02 V vs Ag/AgCl. Spatially resolved equipotential images extracted from the potentiodynamic SECCM movie (Movie S4) are shown at (a) 0.02 V for cycle 1 and

(b) 0.20 V for cycle 2. Corresponding Glucose oxidation-I CVs are shown in (c) for cycle 1 and (d) for cycle 2. See Section 2.3 of the main manuscript for details.

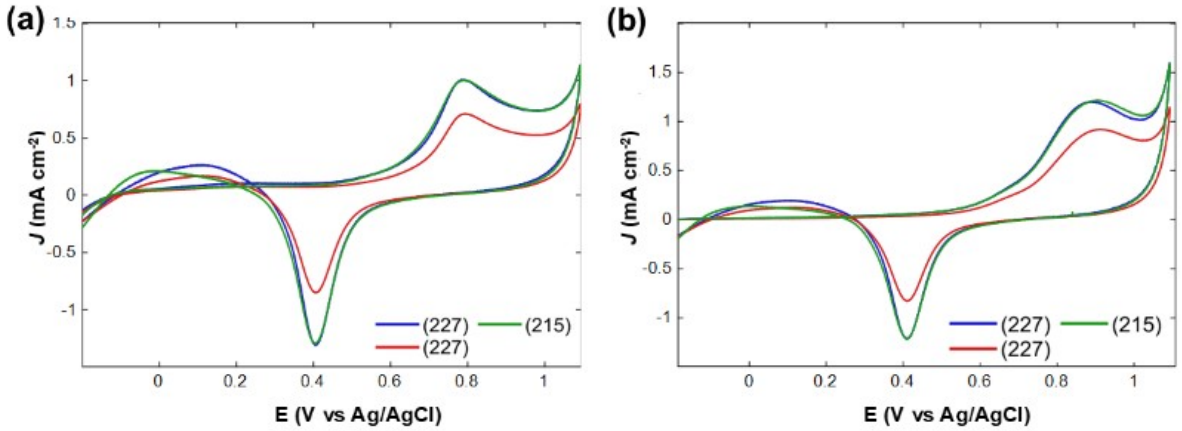

Figure S13. Cyclic voltammograms of glucose oxidation potential 0.08 V vs Ag/AgCl recorded during Glucose Scan 3, showing (a) cycle 1 and (b) cycle 2.

S9. Plausible GOR pathway on polycrystalline gold.

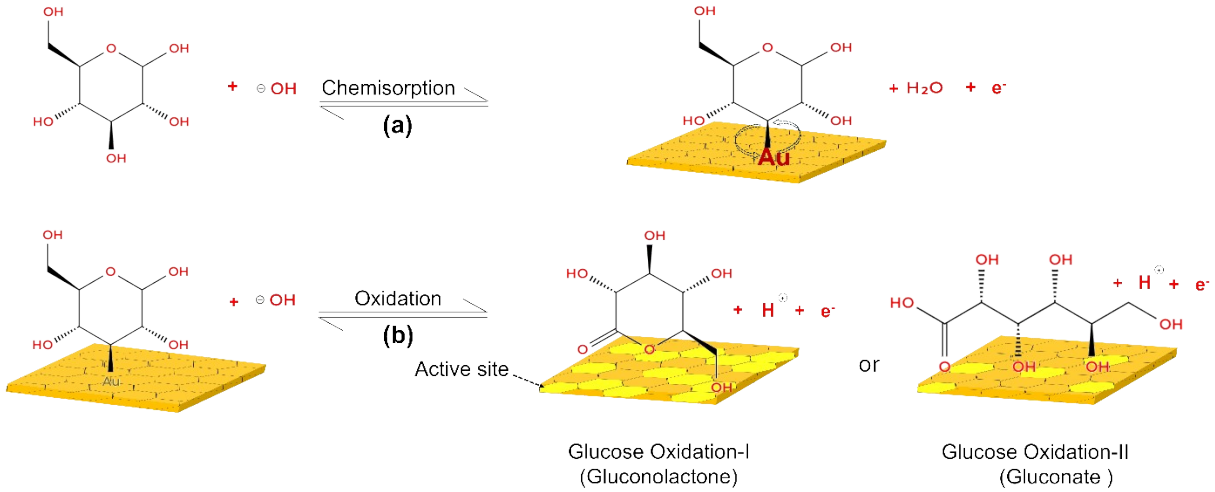

Figure S14. Plausible GOR pathway on polycrystalline gold. (a) Chemisorption of glucose on the gold surface. (b) Oxidation at regions with higher Au active-site density associated with different grain orientations follows Glucose Oxidation-I, yielding gluconolactone, whereas oxidation at regions with lower active-site density follows Glucose Oxidation-II, yielding gluconate.

Reference

1. X. Xu, M. Kang, S. Yan, E. Daviddi, G. West, D. Valavanis, O. J. Wahab and P. R. Unwin, *ACS Electrochem.*,2025, **9**, 1852-1862.
2. R. G. Mariano, M. Kang, O. J. Wahab, I. J. McPherson, J. A. Rabinowitz, P. R. Unwin and M. W. Kanan, *Nat. Mater.,* 2021, **20**, 1000–1006.
3. I. M. Ornelas, P. R. Unwin and C. L. Bentley, *Anal. Chem*., 2019, **91**, 14854–14859.
4. C. L. Bentley, D. Perry and P. R. Unwin, *Anal. Chem.*, 2018, **90**, 7700–7707.
5. O. J. Wahab, M. Kang, E. Daviddi, M. Walker and P. R. Unwin, *ACS Catal.*, 2022, **12**, 6578–6588.
6. C. H. Chen, L. Jacobse, K. McKelvey, S. C. S. Lai, M. T. M. Koper and P. R. Unwin, *Anal. Chem.*, 2015, **87**, 5782–5789.
7. I. T. McCrum, C. J. Bondue and M. T. M. Koper, *J. Phys. Chem. Lett.*, 2019, **10**, 6842–6849.
8. J. H. Shim, J. Kim, A. Go, C. Lee and Y. Lee, *Mater. Lett.*, 2013, **91**, 330–333.
9. H. Seong, M. Oh, K. Jin and D. K. Lee**,** *ACS Energy Lett.***,** 2025**, 10,** 5373–5382**.**